Nanoscale

Cite this: *Nanoscale*, 2012, **4**, 5316

www.rsc.org/nanoscale

COMMUNICATION

Facile control of intra-fiber porosity and inter-fiber voids in electrospun fibers for selective adsorption†

Jinyou Lin,[abcd] Feng Tian,[b] Yanwei Shang,[acd] Fujun Wang,[d] Bin Ding*[ac] and Jianyong Yu*[c]

Received 17th June 2012, Accepted 17th July 2012
DOI: 10.1039/c2nr31515g

We report a facile method to control intra-fiber porosity *via* varying the relative humidity and inter-fiber voids through the blending of two different polymeric fibers *via* multi-nozzles spinning of electrospun fibers for selective adsorption of oil from water.

Over the past few decades, the clean-up of oil from environmental water has been a challenge due to various oil spill accidents, as well as discarded oil products, and water contaminated by oil can greatly damage human health and the environment.[1] Current methods of oil spill clean-up can be categorized into three main types: physical methods (*i.e.*, sorbents, booms, and skimmers), chemical methods (*i.e.*, *in situ* burning and the use of solidifiers), and bioremediation. The mechanical recovery of oil through the use of sorbents is a very common and promising technique.[2,3] In the recovery process, the floating oil is concentrated and transformed from a liquid to a semi-solid or to the solid phase, which can thus be removed using an oil sorbent.[4,5]

The traditional oil sorbent materials include natural fibers, such as cotton,[6] cotton grass fibers,[7] milkweed,[4] kenaf,[4] vegetable fibers,[8] kapok,[9] wool[10] and silkworm cocoon waste,[11] *etc.* Some synthetic fibers, such as polypropylene (PP),[6] have also been used as oil sorbents due to their good hydrophobic–oleophilic properties, high buoyancy, and scalable fabrication. However, PP fibers, as a good candidate for oil sorbents, suffered from a low oil sorption capacity due to its large fiber diameter and nonporous structure.[12] Although most natural sorbents have larger oil sorption capacities than synthetic ones, they often sorb water well, which is a disadvantage when used to remove oil from environmental water. Sometimes their hydrophobicity is enhanced by various post-treatments, but the overall costs of the sorbents is subsequently increased.[7] Therefore, an ideal oil sorbent should have good hydrophobicity–oleophilicity properties, a high uptake capacity, a high rate of uptake, and good buoyancy.[13]

A hydrophobic–oleophilic surface is indispensable for a good oil sorbent with oil–water selectivity. In general, surfaces can be wetted by a liquid with a comparable surface tension and similar polarity; therefore, sorbent surfaces should be nonpolar with a surface tension comparable to oil.[14] To increase the sorption capacity of sorbent materials, porosity can be introduced into the materials, which can provide a higher surface area for oil adsorption. With this aim in mind, many synthetic oil sorbent materials have been synthesized *via* porous materials with high surface areas and porosities, following surface modification using low surface energy materials.[3,15,16] For instance, Liang *et al.*[16] synthesized a new class of hydrogel–aerogels consisting of highly uniform carbonaceous nanofibers coated with polydimethysiloxane, which exhibited a good oil adsorption ability.

Undoubtedly, creating a porous structure using materials with low surface energy in one-step is an efficient and economic way to obtain oil sorbents. In recent years, electrospinning, as an efficient and simple method for producing polymeric fibers with diameters both on micro- and nano-scales, has gained increasing attention due to its unique advantages, such as the variety of materials that can be electrospun into fibers, the fine structures of both the fibers and their assembles, which may be regulated, the multivariate techniques that can be combined with electrospinning and the extendable processing of fiber generation, compared to other processing techniques for micro- and/or nano-fiber generation.[17–21]

Therefore, the fabrication of a porous fibrous mat, composed of micro- and/or nano-fibers, possessing a porous structure within itself *via* nonpolar polymers with a low surface energy is a promising way to generate oil sorbents. It is believed that the oil sorption capacity can be increased if the fibrous sorbent has the capability of driving oil not only into the inter-fiber voids among the fibers, but also to the interior of the fibers, which has a porous structure. In this

[a]*State Key Laboratory for Modification of Chemical Fibers and Polymer Materials, College of Materials Science and Engineering, Donghua University, Shanghai 201620, China. E-mail: binding@dhu.edu.cn; Fax: +86-21-62378202; Tel: +86-21-62378202*
[b]*Shanghai Institute of Applied Physics, Chinese Academy of Sciences, Shanghai 201204, China*
[c]*Nanomaterials Research Center, Research Institute of Donghua University, Shanghai 200051, China. E-mail: yujy@dhu.edu.cn*
[d]*College of Textiles, Donghua University, Shanghai 201620, China*

† Electronic supplementary information (ESI) available: FE-SEM images, nitrogen physisorption isotherms, differential pore volume *vs.* pore width, SAXS 2D scattering patterns and SAXS curves of PS (M_w = 208 000 g mol^{-1}) fibrous mats formed at different RH (Fig. S1). Iron element distribution of a single fiber (Fig. S2). A schematic diagram to show the multi-nozzles electrospinning (Fig. S3). FE-SEM images of as-prepared fibrous mats formed with various PS/PU nozzle ratios (Fig. S4). Nitrogen physisorption isotherms, SSA, and water contact angles of as-prepared fibrous mats formed with various PS/PU nozzle ratios (Fig. S5 and S6). Hydrophobicity–oleophilicity of an as-spun fibrous mat (Fig. S7). Typical tensile stress–strain curves of various PS fibrous mats with the addition of PU fibers formed from a 50 wt% PU resin (Fig. S8). Surface characterization of as-prepared fibers (Table S1). Tensile properties of the fibrous mats (Tables S2 and S3). See DOI: 10.1039/c2nr31515g

communication, we report a facile and direct method to fabricate microfibers with a controllable porous structure *via* electrospinning polystyrene (PS), a nonpolar polymer with a low surface energy, in solution for selective adsorption.

In electrospinning, the relative humidity (RH) plays an important role in the formation of fiber structures due to its effect on the phase separation and solidification of the fluid jet.[17] Fig. 1a and b show FE-SEM images of PS fibers formed at different RHs while the other parameters were kept constant (further details are shown in the ESI†). As can be seen, the fibers formed at a RH of 45% show very smooth surfaces with an average diameter of 2.86 μm; whereas the fibers formed at 20% RH exhibit relatively rough surfaces and a large diameter deviation with an average diameter of 0.97 μm. Furthermore, the inset in Fig. 1a indicates the fiber has a highly porous interior encapsulated by a very thin skin; however, the fiber cross-section shown in Fig. 1b presents a solid fiber interior instead of a porous core. This demonstrates that the high RH enables a large intra-fiber porosity to be obtained within the PS fiber *via* electrospinning.

The intra-fiber porosity can be explained by the competition between the phase separation and the solidification of the fluid jet during electrospinning. Usually, the phase separation is induced by solvent evaporation and vapor precipitation within the fluid jet, which constitutes the thermally-induced phase separation and the vapor-induced liquid–liquid phase separation.[22–24] A high RH allows much more vapor in the air to penetrate the fluid jet and induces phase separation, which leads to the formation of intra-fiber porosity. Therefore, under very low RH conditions, there is too little vapor in the air to penetrate the fluid jet, triggering phase separation; thus, a solid interior is formed within the fiber. Under such low RH conditions, jet solidification is delayed and the fibres become thinner, eventually leading to capillary instability,[24] which results in the formation of thinner fibers with rough surfaces (Fig. 1b).

To characterize the intra-fiber porosity, the nitrogen physisorption method was used. Fig. 1c and d show the nitrogen adsorption–desorption isotherms of the PS fibers prepared at different RHs. As can be seen, the former fibers (RH = 45%) have a maximal nitrogen adsorption capacity of 282.19 $cm^3\ g^{-1}$, which is approximately 58 times that of the fibers formed at 20% RH, indicating large intra-fiber porosity existing within the fibers. The PS fibers formed at 45% RH show a specific surface area (SSA) of 50.63 $m^2\ g^{-1}$; however, the fibers formed at 20% RH only have a SSA of 4.09 $m^2\ g^{-1}$, which is an increase of at least a factor of 12 as compared to the fibers formed at 45% RH. Furthermore, the total pore volume (TPV) of the former fibers (0.427 $cm^3\ g^{-1}$) is 61 times that of the latter fibers (0.007 $cm^3\ g^{-1}$) (Table S1†).

As shown in Fig. 1c and d, the nitrogen physisorption isotherms show a type II isotherm with a hysteresis loop, indicating the existence of mesopores (2–50 nm) and macropores (>50 nm) within the fibers.[25] The inset in Fig. 1c presents the differential pore volume *vs.* the pore width calculated by applied density functional theory (DFT) to the adsorption isotherm, which shows that the pores range from 20 nm to 120 nm; however, the pores within the PS fibers formed at 20% RH show two peaks centered at 13 nm and 37 nm (inset in Fig. 1d). It should be noted that the ordinate value in the inset of Fig. 1d is two orders of magnitude smaller compared with the inset in Fig. 1c, demonstrating that there are very few pores within the fibers implying a very small total pore volume, which is in good agreement with the results shown in Table S1.†

To further investigate the nanoscale structure and structural fluctuations within the as-prepared fibers, small-angle X-ray scattering (SAXS) was performed on beamline BL16B1 of the Shanghai Synchrotron Radiation Facility (SSRF). Fig. 1e presents the SAXS 2D scattering patterns and SAXS curves of the as-prepared fibers at different RHs. Obviously, the scattering pattern of the fibers formed at 45% RH shows a circular shape, indicating the nanoscale structure that is randomly oriented within the fibers. In addition, the shape is larger than that of the fibers formed at 20% RH and, as a result, a more complicated nanoscale structure is presented within the former fibers, representing a larger intra-fiber porosity. The SAXS curves of these fibers obtained from SAXS 2D scattering data through integrating in the range of −45° to +45° clearly illustrates the difference in the intra-fiber porosity of these fibers. This concludes that the intra-fiber porosity can be easily manipulated by changing the RH during electrospinning. A further demonstration of this is also shown in Fig. S1 and Table S1.†

The nonpolar and low surface energy of PS enabled the electrospun PS microfibers to have good hydrophobicity, or even superhydrophobicity, due to the addition of hierarchical structures.[26] Furthermore, the inherent properties of PS also make it oleophilic. To evaluate the effect of the intra-fiber porosity on oil adsorption, we compared the oil sorption capacity of a single fiber formed at

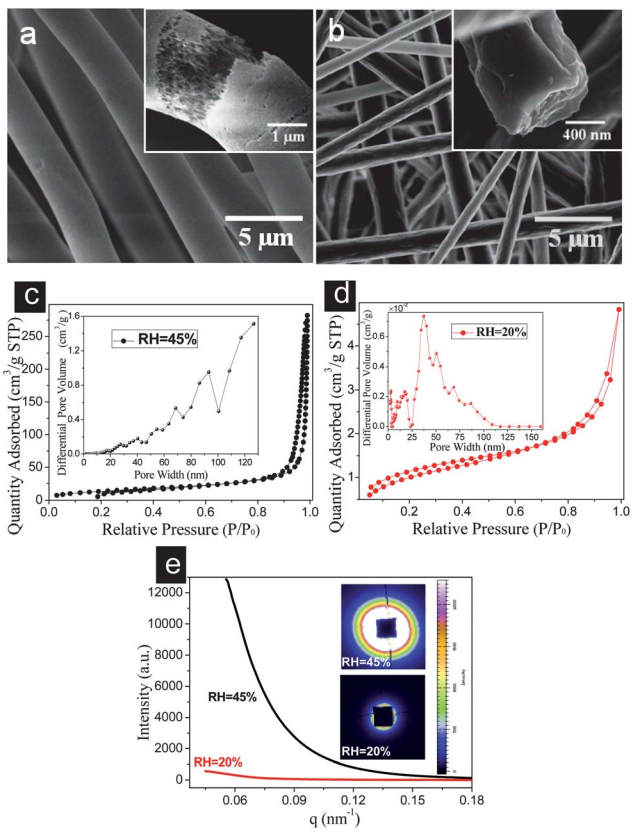

Fig. 1 FE-SEM images of fibrous mats formed from a 20 wt% PS (M_w = 350 000 g mol^{-1}) solution at a RH of (a) 45% and (b) 20%. Nitrogen adsorption–desorption isotherms and differential pore volume *vs.* pore width of the as-prepared fibers formed at a RH of (c) 45% and (d) 20%. (e) Small-angle X-ray scattering (SAXS) 2D scattering patterns and SAXS curves of as-prepared fibers formed at different RHs. (Fit2D software was used to analyze the 2D SAXS data.)

different RHs qualitatively. Fig. 2a and c show single PS fibers taken from the samples shown in Fig. 1a and b, respectively, which were placed on a copper wire mesh after oil sorption with a traceable element (iron). The insets of Fig. 2a and c show the scanning transmission X-ray microscopy (STXM) images of oil sorbed fibers performed on a BL08U1A microscope at the SSRF. Fig. 2b and d show the distribution of iron within the single fiber, which was calculated using software from the Dual Energy Element Distribution,[27] illustrating that there is much more iron distributed within the fiber with a larger intra-fiber porosity. Fig. S2b† shows the iron distribution within the fiber formed at 20% RH with a different magnification, showing no obvious difference from Fig. 2d and indicating that only a very little oil was sorbed by the nonporous PS fiber prepared under these conditions.

The dotted yellow circles in Fig. 2a represent the different areas that were scanned and the corresponding iron distributions are shown in Fig. 2b and Fig. S2a,† respectively. If oil can not penetrate through the thin skin layer of the fiber to reach the porous core (Fig. S2a†), more iron will be evident on the surface of the fiber. However, we note that the iron distribution of the two different areas highlighted in Fig. 2a are similar. Therefore, the thin skin surrounding the porous core does not appear to effect the oil sorption. Fig. S2c and S2d† show the iron distributions of the single fiber formed at different RHs after washing with deionized water containing a detergent to remove the sorbed oil from the fiber surface. As can be noted, iron was still present in the case of the porous fiber, while it was almost completely removed from the solid fiber. This result shows that the fiber formed at 20% RH only sorbs the oil on its surface due to its nonporous structure, which agrees very well with the results obtained from the nitrogen physisorption study.

It was found that the PS fibers (using the fiber assembly as a mat) formed at 45% RH have oil sorption capacities of 113.87 g g^{-1} and 96.89 g g^{-1} for motor oil and sunflower seed oil, respectively, in accordance with our previous report.[28] However, the fibers formed at 20% RH show oil sorption capacities of 64.80 g g^{-1} and 67.45 g g^{-1} for these same two oils. Similar results were also obtained for the fibers formed from a 30 wt% PS (M_w = 208 000 g mol^{-1}) solution at different RH as shown in Fig. S1.† For 45% RH, the fibers show oil sorption capacities of 84.41 g g^{-1} and 79.62 g g^{-1} for motor oil and sunflower seed oil, whereas, the fibers formed at 20% RH have oil sorption capacities of 47.72 g g^{-1} and 40.59 g g^{-1}. Therefore, it can be concluded that the oil sorption capacities of the fibers is predominantly influenced by inter-fiber voids rather than intra-fiber porosity.

Although the PS fibrous mats, which were three-dimensional (3D) networks composed of microfibers with high intra-fiber porosity, showed a comparatively high oil sorption capacity in comparison with oil sorption material reported in previous publications, they suffered from a fatal problem: poor mechanical strength of the oil adsorbed fibers, which prevented their reuse. The intra-fiber porosity provided a much greater area for oil anchoring; however, the shape could not be recovered after squeezing to recycle the adsorbed oil, which is likely to be due to the poor elasticity of PS.

To improve the mechanical properties, in particular the elasticity and recoverability of the as-prepared fibrous mats, we added some electrospun polyurethane (PU) fibers, which have a good tensile strength and elongation,[29] to the fibrous mats to regulate the inter-fiber voids and enhance the mechanical properties *via* multi-nozzles electrospinning of the different polymer solutions as shown in Fig. S3.† Fig. 3a and b show the FE-SEM images of the fibrous mats formed from a 20 wt% PS (M_w = 350 000 g mol^{-1}) solution at a RH of 45% with different PS/PU nozzle ratios. As shown in the insets of Fig. 3a and b, the PS fibers have smooth surfaces with porous

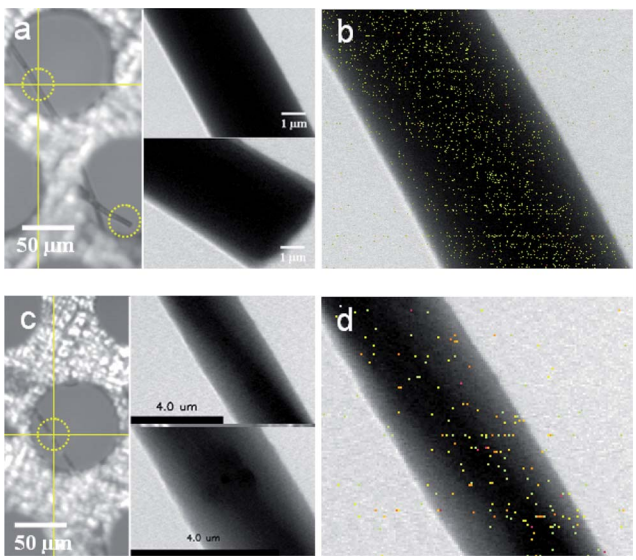

Fig. 2 (a) and (c) show single PS fibers taken from the samples shown in Fig. 1a and b, respectively, which were placed on a copper wire mesh after oil sorption. (b) and (d) Iron distribution within the single fibers shown in (a) and (c), respectively. (The insets of (a) and (c) show the STXM images of the corresponding fiber with different areas and the smallest pixel size from top to bottom as follows: 8 μm × 8 μm, 25 nm; 10 μm × 10 μm, 40 nm; 8 μm × 8 μm, 50 nm; 5 μm × 5 μm, 25 nm. The yellow dotted circle indicates the position of the scan.)

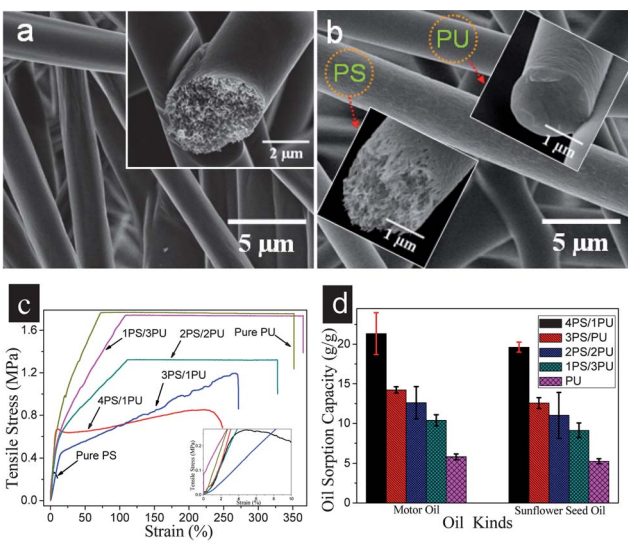

Fig. 3 FE-SEM images of the fibrous mats formed from a 20 wt% PS (M_w = 350 000 g mol^{-1}) solution at a RH of 45% with different nozzle ratios of PS/PU: (a) 4/1, (b) 3/1. (The insets show a cross-section of the as-prepared fibers.) (c) Typical tensile stress–strain curves and (d) the oil sorption capacities of the as-spun fibers formed with various nozzle ratios of PS/PU. (4PS/1PU represents a nozzle ratio of PS to PU of 4/1; PU was the initial resin.)

interiors, while the PU fiber exhibits a smooth surface with a solid interior. Additional FE-SEM images of the as-prepared fibrous mats formed with various PS/PU nozzle ratios are shown in Fig. S4.† It can be found that, as the density of PU fibers is increased in the composite fibrous mats, the fibrous mats begin to pack closely, suggesting a reduction in the inter-fiber voids among the fibers.

Fig. 3c shows the typical tensile stress–strain curves of the as-prepared fibrous mats. The stress–strain curve of a pure PS fibrous mat is approximately linear up to the yield point (inset in Fig. 3c), which follows an initial period with a steep slope. In the initial period, the fibers were subjected to an increasing load and they began to endure the main load after the slip was completed. Because of intra-fiber porosity, the PS fibers exhibited very poor extension and strength and broke after the yield point. However, the stress–strain curve of the pure PU fibrous mat showed an initial period with a steep slope, with the strain then easing and increasing until breakage occurred while the stress remained almost constant (Fig. 3c). This deformation can be attributed to the good mechanical property of the solid electrospun PU fibers, as well as the mutual adhesion of the PU fibers due to the residual solvent and hydrogen bonds in the PU molecule chains. As shown in Fig. 3c and Table S2,† the pure PS fibrous mat showed very low tensile strength (0.26 MPa) and elongation at the breaking point (4.99%), whereas the pure PU fibrous mat showed a breaking strength of 1.76 MPa and an elongation at the breaking point of 108.65%. The composite fibrous mat formed with a PS/PU nozzle ratio 4/1 showed a tensile strength of 0.84 MPa and an elongation at the breaking point of 223.37%. This demonstrated that the mechanical properties of the as-prepared fibrous mats can be efficiently improved *via* multi-nozzles electrospinning.

The electrospun PU fibers are solid with a very small SSA and are hydrophilic due to the existence of amide groups in the PU molecular chain. Therefore, the SSA and water contact angles (WCAs) of the fibrous mats will decreased with an increase of the PU content in the composite fibrous mats, as shown in Fig. S5 and S6.† This shows that the water droplets can be stably placed on the fibrous mats and exhibit a large WCA, while the oil droplets are adsorbed by the fibrous mat after about ten seconds (Fig. S7†). Fig. 3d shows the oil sorption capacities of the various fibrous mats with regards to motor oil and sunflower seed oil and shows that the oil sorption capacities for both the oils decreases as the PU content is increased in the fibrous mats. It can also be found that the addition of electrospun PU fibers to the PS fibers with intra-fiber porosity enabled the oil sorption capacities to be dramatically reduced, which was mainly attributable to the decreasing of the inter-fiber voids among the fibers through the blending of the two different fibers.

To further decrease the PU fibers in composite fibrous mats, the PS/PU nozzle ratio was kept constant at 4/1 and the initial PU resin was diluted to 50 wt% in the spinning solution. Fig. 4a and b show the FE-SEM images of the fibrous mats formed at a RH of 45% from different PS solutions. As can be seen, the diameter of the PU fibers is significantly reduced (less than 1 μm) due to a decrease in the solution concentration and the cross-section of the PS fibers shows highly porous interiors. Because of the reduction of the PU fibers in the composite fibrous mats, their SSA and TPV increase as compared to the corresponding fibrous mats formed with an initial PU resin (Table S1†). Although the PU fiber content was decreased, both the tensile strength and elongation at the breaking point improved significantly in comparison to the pure PS fibers (Table S3†). In addition, the fibrous mat formed from a 30 wt% PS solution showed

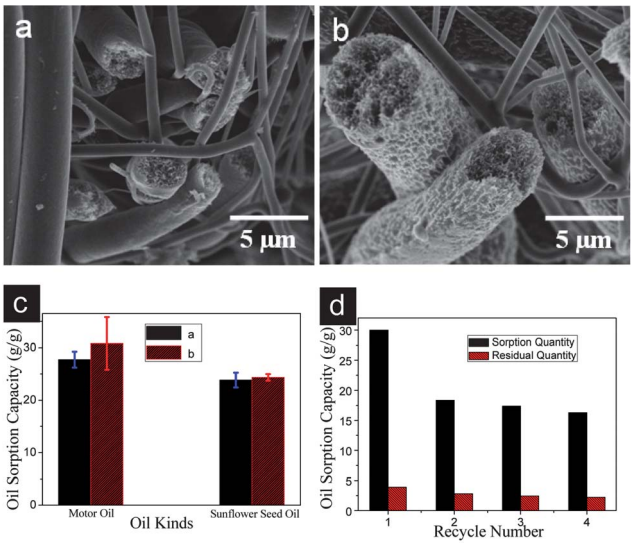

Fig. 4 FE-SEM images of fibrous mats formed at a RH of 45% with a 4/1 PS/PU nozzle ratio from different PS solutions: (a) 20 wt% PS (M_w = 350 000 g mol^{-1}), (b) 30 wt% PS (M_w = 208 000 g mol^{-1}). (c) Oil sorption capacities of the corresponding fibers shown in (a) and (b). (d) Reusability of the fibrous mat shown in (b). (A 50 wt% PU resin was used.)

a poor elongation compared with that formed from a 20 wt% PS solution due to more fibers being generated from the 30 wt% solution under the same conditions (Fig. S8†).

Fig. 4c shows the oil sorption capacities of these two fibrous mats for motor oil and sunflower seed oil. As can be seen, the fibrous mat shown in Fig. 4a has oil sorption capacities of 27.75 g g^{-1} and 23.84 g g^{-1} for these two oils, which are 6.41 g g^{-1} and 4.21 g g^{-1} higher than that of the fibrous mat formed from the same PS solution using an initial PU resin. This result indicates that the oil sorption capacities of as-prepared fibrous mats increases as the PU fibers content decreases in the composite fibrous mats. The fibrous mat shown in Fig. 4b shows oil sorption capacities of 30.81 g g^{-1} and 24.36 g g^{-1} for these two oils, which is much higher than that of the fibrous mat shown in Fig. 4a, which can be ascribed to the presence of more PS fibers in this composite fibrous mat.

As shown in Fig. 4d, the fibrous mat has a 29.98 g g^{-1} oil sorption capacity for motor oil. The fibrous mat with oil was squeezed by a padding paper at the maximum pressure to remove the sorbed oil. There was still 3.90 g g^{-1} residual oil within the squeezed fibrous mat. When the fibrous mat was used for a second time, its oil sorption capacity and residual oil quantity were 18.36 g g^{-1} and 2.82 g g^{-1}, respectively. The oil sorption capacity decreased each time the mat was reused. The drop in the oil sorption capacity following the first reuse was larger than that of the second reuse, which was comparatively small. This may be due to the irreversible deformation of the as-prepared fibrous mat. It is worth noting that the fibrous mat still maintained a comparable oil sorption capacity of surface modified nanowire membranes (18.56 g g^{-1})[15] and wool-based nonwoven fibers (17.24 g g^{-1})[30] after several cycles, which is approximately 30 times that of flaxseed gum gel beads with regards to mineral oil (0.55 g g^{-1}).[31]

In summary, we have reported a facile method to control the intra-fiber porosity and inter-fiber voids in electrospun fibers for oil–water selective adsorption. The results demonstrate that intra-fiber porosity can be easily controlled by varying the RH during electrospinning, while the inter-fiber voids among the fibers can be manipulated by

blending the two different polymer fibers *via* multi-nozzle electrospinning. Oil sorption tests indicated that the oil sorption of a single fiber was overwhelmingly governed by the intra-fiber porosity and the oil sorption capacity of the fiber assembly was predominantly determined by the inter-fiber voids over the intra-fiber porosity. The mechanical properties of the as-prepared fibrous mats have been significantly improved by blending with elastic PU fibers, which enabled the fibrous mats to be reused. We believe that electrospun fibers with versatile structures, such as a core–shell, side-by-side, helix or hollow structure, that possess high porosity and SSA will have potential applications in selective adsorption and separation.

Acknowledgements

This work was supported by the National Basic Research Program of China (973 Program, 2011CB606103 and 2012CB525005), the National Natural Science Foundation of China (No. 51173022), the "111 Project" (No. 111-2-04 and B07024), the Shanghai Committee of Science and Technology (No. 10JC1400600), the Shanghai Nano Special Projects (11nm0502900), the Innovation Program of Shanghai Municipal Education Commission (11ZZ59), the "Dawn" Program of Shanghai Education Commission (10SG32), the Scientific Research Foundation for the Returned Overseas Chinese Scholars, Ministry of Education of China, the Program for New Century Talents of the University in China, and the Fundamental Research Funds for the Central Universities. We thank beamline BL16B1 and BL08U of SSRF for providing the beam time. As the first author, I would like to thank Dr Jie Wang, Dr Xiuhong Li, Dr Zhi Guo and Dr Lijuan Zhang for their helpful discussions.

Notes and references

1 M. Fingas, *Oil Spill Science and Technology: Prevention, Response, and Clean Up*, Gulf Professional Publishing, 2010.
2 A. Bayat, S. F. Aghamiri, A. Moheb and G. R. Vakili-Nezhaad, *Chem. Eng. Technol.*, 2005, **28**, 1525–1528.
3 J. T. Korhonen, M. Kettunen, R. H. A. Ras and O. Ikkala, *ACS Appl. Mater. Interfaces*, 2011, **3**, 1813–1816.
4 H. M. Choi and R. M. Cloud, *Environ. Sci. Technol.*, 1992, **26**, 772–776.
5 Q. Wei, R. Mather and A. Fotheringham, *Bioresour. Technol.*, 2005, **96**, 331–334.
6 H. M. Choi, H. J. Kwon and J. P. Moreau, *Text. Res. J.*, 1993, **63**, 211–218.
7 S. Suni, A. L. Kosunen, M. Hautala, A. Pasila and M. Romantschuk, *Mar. Pollut. Bull.*, 2004, **49**, 916–921.
8 T. R. Annunciado, T. H. Sydenstricker and S. C. Amico, *Mar. Pollut. Bull.*, 2005, **50**, 1340–1346.
9 T. T. Lim and X. Huang, *Chemosphere*, 2007, **66**, 955–963.
10 V. Rajakovic, G. Aleksic, M. Radetic and L. Rajakovic, *J. Hazard. Mater.*, 2007, **143**, 494–499.
11 H. Moriwaki, S. Kitajima, M. Kurashima, A. Hagiwara, K. Haraguchi, K. Shirai, R. Kanekatsu and K. Kiguchi, *J. Hazard. Mater.*, 2009, **165**, 266–270.
12 Q. Wei, *Mar. Pollut. Bull.*, 2003, **46**, 780–783.
13 D. Ceylan, S. Dogu, B. Karacik, S. D. Yakan, O. S. Okay and O. Okay, *Environ. Sci. Technol.*, 2009, **43**, 3846–3852.
14 R. Wenzel, *Ind. Eng. Chem.*, 1936, **28**, 988–994.
15 J. Yuan, X. Liu, O. Akbulut, J. Hu, S. L. Suib, J. Kong and F. Stellacci, *Nat. Nanotechnol.*, 2008, **3**, 332–336.
16 H. W. Liang, Q. F. Guan, L. F. Chen, Z. Zhu, W. J. Zhang and S. H. Yu, *Angew. Chem., Int. Ed.*, 2012, **51**, 5101–5105.
17 D. Li and Y. N. Xia, *Adv. Mater.*, 2004, **16**, 1151–1170.
18 R. Nirmala, R. Navamathavan, H. S. Kang, M. H. El-Newehy and H. Y. Kim, *Colloids Surf., B*, 2011, **83**, 173–178.
19 X. F. Wang, B. Ding, J. Y. Yu and M. R. Wang, *Nano Today*, 2011, **6**, 510–530.
20 J. Du, P. L. Che, Z. Y. Wang, U. Aich and K. J. Yarema, *Biomaterials*, 2011, **32**, 5427–5437.
21 J. Y. Lin, X. F. Wang, B. Ding, J. Y. Yu, G. Sun and M. Wang, *Crit. Rev. Solid State Mater. Sci.*, 2012, **37**, 94–114.
22 P. Dayal, J. Liu, S. Kumar and T. Kyu, *Macromolecules*, 2007, **40**, 7689–7694.
23 J. Y. Lin, B. Ding, J. M. Yang, J. Y. Yu and G. Sun, *Nanoscale*, 2012, **4**, 176–182.
24 C. L. Pai, M. C. Boyce and G. C. Rutledge, *Macromolecules*, 2009, **42**, 2102–2114.
25 K. Sing, D. Everett, R. Haul, L. Moscou, R. Pierotti, J. Rouquerol and T. Siemieniewska, *Pure Appl. Chem.*, 1985, **57**, 603–619.
26 B. Ding, J. Y. Lin, X. F. Wang, J. Y. Yu, J. M. Yang and Y. Cai, *Soft Matter*, 2011, **7**, 8376–8383.
27 X. Zhang, Z. Xu, R. Tai, X. Zhen, Y. Wang, Z. Guo, R. Yan, R. Chang, B. Wang and M. Li, *J. Synchrotron Radiat.*, 2010, **17**, 804–809.
28 J. Y. Lin, Y. W. Shang, B. Ding, J. M. Yang, J. Y. Yu and S. S. Al-Deyab, *Mar. Pollut. Bull.*, 2012, **64**, 347–352.
29 R. Sen, B. Zhao, D. Perea, M. E. Itkis, H. Hu, J. Love, E. Bekyarova and R. C. Haddon, *Nano Lett.*, 2004, **4**, 459–464.
30 M. Radetic, V. Ilic, D. Radojevic, R. Miladinovic, D. Jocic and P. Jovancic, *Chemosphere*, 2008, **70**, 525–530.
31 J. J. Long, Y. G. Zu, Y. F. Fu, M. Luo, P. S. Mu, C. J. Zhao, C. Y. Li, W. Wang and J. Li, *RSC Adv.*, 2012, **2**, 5172–5177.

